JACS
JOURNAL OF THE AMERICAN CHEMICAL SOCIETY
Article
pubs.acs.org/JACS

Inorganic Nanostructures with Sizes down to 1 nm: A Macromolecule Analogue

Shi Hu, Huiling Liu, Pengpeng Wang, and Xun Wang*

Department of Chemistry, Tsinghua University, Beijing, 100084, P. R. China

Supporting Information

ABSTRACT: Ultrathin nanostructures exhibit many interesting properties which are absent or less-pronounced in traditional nanomaterials of larger sizes. In this work, we report the synthesis of ultrathin nanowires and nanoribbons of rare earth hydroxides and demonstrate some new phenomena caused by their atomic-level lateral size (1 nm), including ligand-induced gelation, self-assembly framework, and conformational diversity. These features are typically, although not exclusively, found in polymer solutions. The properties of the inorganic backbone and the emerging polymeric characteristics combined prove to be very promising in the design of new hybrid materials.

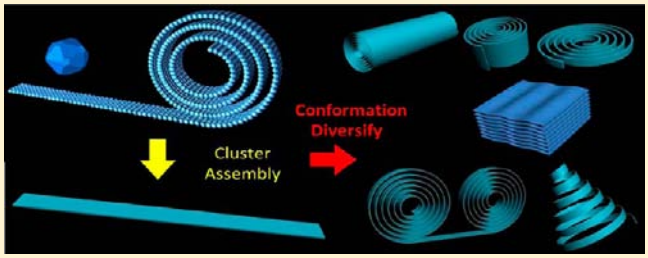

INTRODUCTION

The past 30 years have witnessed the blossom of nanoscience owing to the fascinating properties related to the reduced dimensions of inorganic materials.[1−7] Polymers (or macromolecules), on the other hand, represent another class of materials with unique properties such as plasticity, viscoelasticity, etc. as compared to inorganic crystallites and are widely used in packaging, textiles, architecture, and transportation, etc. Previously, scientists studied hybrids of these nanomaterials with different polymers[8−13] to harvest the unique features of both. The characteristic properties of polymers are inherently determined by the conformation of their polymeric chains, which are missing in conventional inorganic nanomaterials. Especially, biomolecules are a group of polymeric molecules with great conformational diversity through which their functions are regulated. One-dimensional (1D) inorganic nanostructures typically do not have these conformational varieties because of limited flexibility as compared to organic molecules. Computer simulation results of 1D ultrathin nanostructures[14] indicate that their atomic arrangement could be significantly different from those of crystalline structures, and this exotic packing was observed in nanotube-templated Ag nanowires by electron microscope.[15] Recent interest in and improvement of the synthesis of colloidal ultrathin nanostructures[16−29] have inspired the idea that 1D ultrathin nanostructures could show similar polymer-like features when they achieve near-atomic dimensions (typically less than 2 nm),[16,23,26,28] while the conformation and growth kinetics of 1.6-nm Bi_2S_3 nanowires were already found to be polymer-analogous.[26] However, progress in this area has been slow with limited new phenomena, partly because of the relatively big size of the investigated nanostructures as compared with the diameter/thickness of polymers or biomolecules.[28,30]

In this paper, we demonstrated the fabrication of new kinds of one-dimensional ultrathin nanostructures (nanowires and nanoribbons) of rare earth hydroxide with diameters/thicknesses less than 1 nm from the assembly of ultrafine nanoclusters. These nanostructures possessed a polymer-comparable size and displayed interesting and controllable conformational diversity. The conformational diversity and tunability were determined by the energy balance between organic ligands, inorganic structure, and solvent, with reduced flexural rigidity of 1D ultrathin nanostructures. In addition, the size reduction of the inorganic nanostructures gave them great similarity to macromolecules: the ultrathin nanowires mimicked the polymeric molecules in wire entanglement, non-Newton rheological behavior, and gelation phenomena, etc; the ultrathin nanoribbons demonstrated interesting conformational diversity and tunability comparable to that of biomolecules. Our preliminary study in this paper showed that 1D inorganic nanomaterials could take on new and macromolecule-like features while retaining their intrinsic characteristics when their size and dimension was carefully controlled around 1 nm, a size comparable with the diameter of a polymer chain (Figure 1b). This could contribute to the design of new kinds of hybrid materials with the combined features of inorganic substrate and various polymers.

EXPERIMENTAL SECTION

Synthesis of Ultrathin Nanowire. In a typical synthesis, 0.4 g of $GdCl_3$ was dissolved in a mixture of 6 mL of ethanol and 0.5 mL of water under ultrasonication, and added into the mixture of 0.89 g of oleic acid (OA) and 1.63 g of oleylamine (OM) with vigorous stirring. After the slurry was further stirred for 10 min, it was sealed in a 10 mL-capacity Teflon-lined autoclave and heated at 170 °C for 4 h. After the

Received: April 8, 2013
Published: July 9, 2013

   dx.doi.org/10.1021/ja403471d | J. Am. Chem. Soc. 2013, 135, 11115−11124

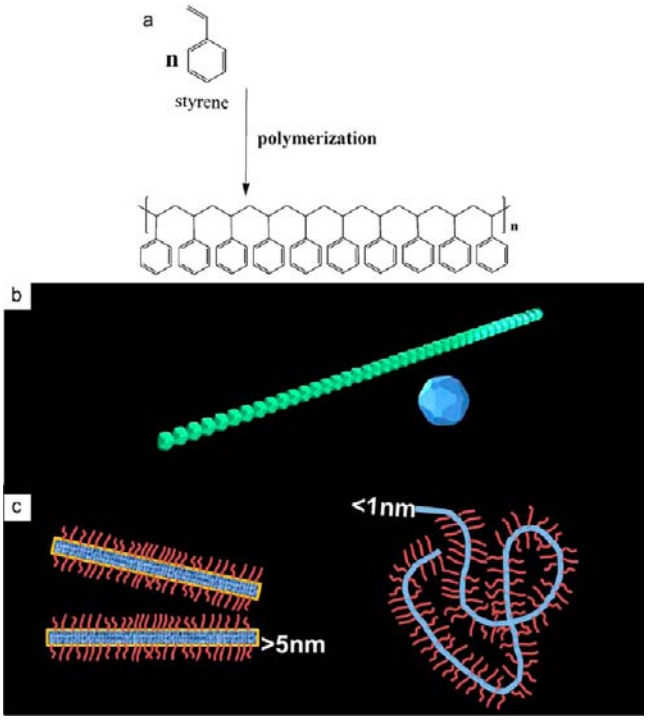

Figure 1. Schematic comparison between the formation of polystyrene and that of one-dimensional ultrathin nanostructures: (a) polystyrene was polymerized from styrene monomers; (b) polymer-like growth model of 1-dimensional nanowire from monomers of tiny nanoclusters; (c) scheme illustrating the conformational difference between rigid thick nanowires (d > 5 nm) and flexible ultrathin nanowires (d < 1 nm).

slurry was cooled to room temperature, the white cake-like product was dispersed in cyclohexane with ultrasonication and violently stirred until no apparent residue could be seen. The product was then precipitated with ethanol and centrifugated at 10000 rpm to remove excess OA and OM. After three cycles of dispersion and wash the final precipitate was dispersed in cyclohexane.

Synthesis of Nanoroll with Medium A.R. In a typical synthesis, 0.196 g of YCl_3 was dissolved in a mixture of 5 mL of ethanol and 0.5 mL of water under ultrasonication, and added into a mixture of 2.7 g of oleic acid (OA) and 0.8 g of oleylamine (OM) with vigorous stirring. After the slurry was further stirred for 10 min, it was sealed in a 10 mL-capacity Teflon-lined autoclave and heated at 180 °C for 4 h. After the slurry was cooled to room temperature, the gel-like product was dispersed in cyclohexane or other nonpolar solvent with ultrasonication, precipitated with ethanol, and centrifugated at 10000 rpm to remove excess OA and OM. After three cycles of dispersion and wash, the final sediment was dried in air. A further step, centrifugation of the cyclohexane dispersion (without ethanol addition) and redispersion of the precipitate, can be done at any time to remove coexisting nanoclusters in the product.

For the synthesis of decoiled nanorolls, temperature and reaction time must be properly increased (details will be discussed in the following parts). For the synthesis of high aspect ratio (AR) long nanorolls, 0.4 g of OA and 2.7 g of OM were used while other materials and conditions remained unchanged. For the synthesis of low AR flat nanorolls, 0.9 g OA and 0.5 g OM were used while other materials and conditions remained unchanged.

Structural Analysis. The X-ray diffraction pattern of the product was conducted on a Rigaku MiniFlex X-ray diffractometer using Cu Kα radiation (λ = 0.154 nm). The final product dispersed in cyclohexane or other solvent was dropped onto a holey copper grid covered with an amorphous carbon film prior to the TEM examination of morphology. Especially, for the characterization of ultrathin nanowires (UTNWs), the product from one batch of reaction was dispersed in 20 mL of cyclohexane and used as the standard solution. It was then diluted to a different concentration, and one drop of the dispersion (diluted 200 times) was dropped onto the copper grid for TEM observation. As for UTNW loops, a further diluted cyclohexane dispersion of UTNWs was mixed with ethanol and then dropped onto the carbon film for TEM observation. The reaction mixture was centrifuged, and the lower-layer liquid was separated, dispersed in cyclohexane, and washed with ethanol. After the mixture was dried in an oven at 70 °C, the product became a waxy sticky solid, as shown in the inset of Figure 5a. To demonstrate its strength, two long steel plates were machined with smooth surfaces and a subgram amount of this glue was pasted between them. The glue was softened by heating and solidified while cooling. Two metallic wires were hung on opposite ends of two plates through machined holes while one wire was also attached to a dumbbell so the dumbbell could be lifted by the other

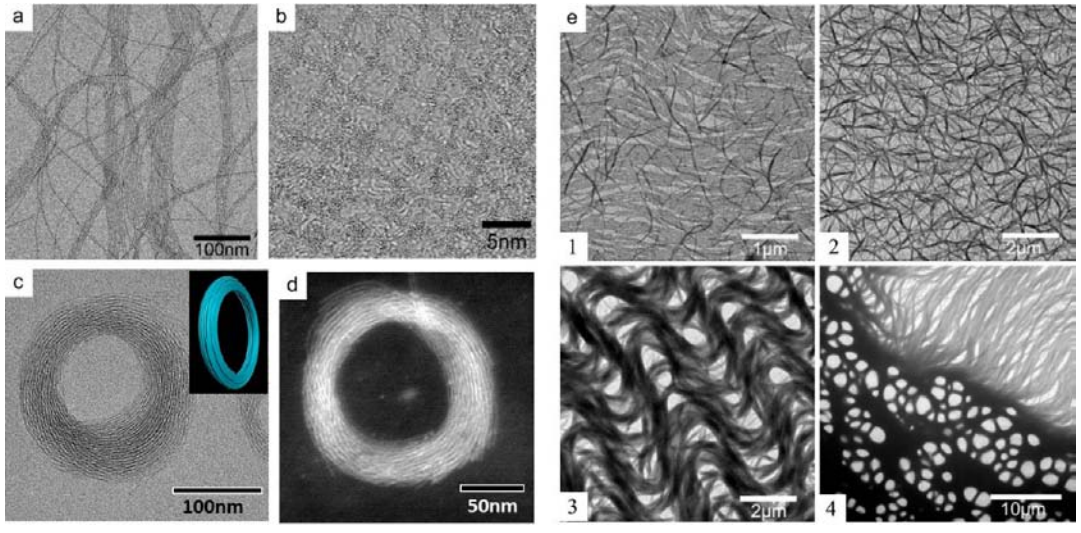

Figure 2. The conformations and assembly behavior of GdOOH UTNWs: (a) TEM images of the UTNWs; (b) HRTEM image of cross-paved UTNWs; (c) TEM and (d) STEM images of UTNW rings prepared from a mixed solvent of cyclohexane and ethanol; (e) subimages 1−4 were a series of TEM images of UTNWs from cyclohexane dispersion with increasing concentration, showing the gradually built framework of entangled NW bundles.

dx.doi.org/10.1021/ja403471d | J. Am. Chem. Soc. 2013, 135, 11115−11124

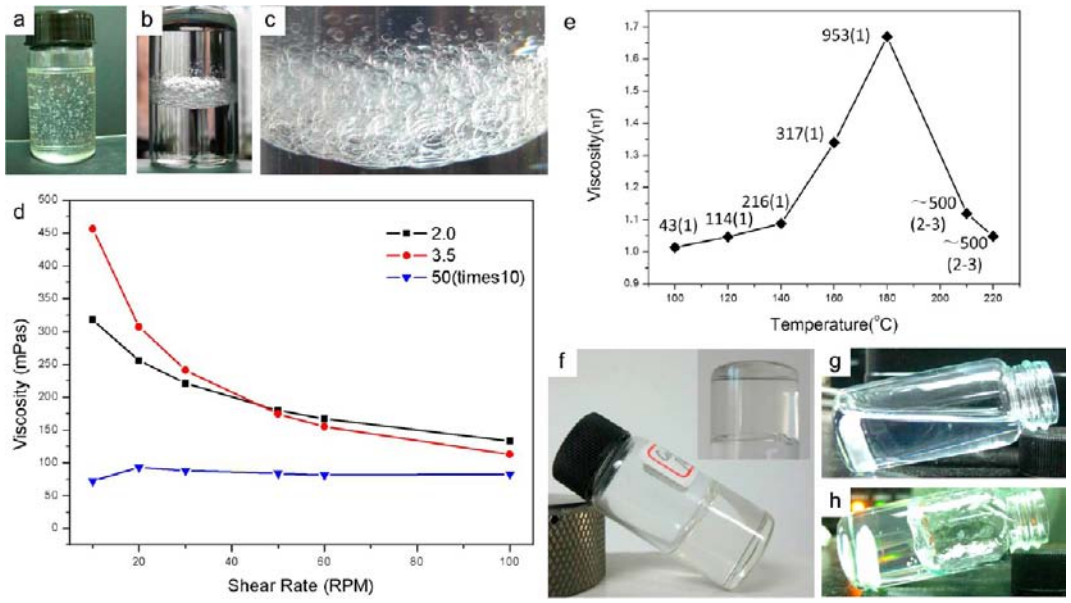

Figure 3. The viscosity and gelation phenomena of cyclohexane dispersion of UTNWs. (a) Photograph of air bubbles trapped in a clear concentrated cyclohexane dispersion of UTNWs. (b) Photograph of extremely stable water droplets trapped at the bottom of a cyclohexane dispersion of UTNWs with an interface-magnified image shown in panel c. (d) Rheological curve from a cyclohexane dispersion of UTNWs with three different concentrations (diluted by 2, 3.5, and 50 times from one standard dispersion), showing Newton fluid behavior only at low concentration and non-Newton fluid behavior at high concentration. (e) Relative viscosity of diluted cyclohexane solution of UTNWs from different reaction temperatures (measured with an Ubbelohde viscometer). The numbers beside the data points showed the corresponding average length of the UTNWs with the radius included in the brackets. (f) Formation of transparent organogel after a 2-day aging period of the concentrated dispersion in open air. (g,h) Photograph of cyclohexane dispersion of UTNWs before and after introduction of naphthylacetic acid (a magnet was fixed in the gel).

wire. For quantitative evaluation of the shear–force, two metal plates were loaded onto the two holders of a Zwick Roell Z020 universal material testing machine and measured under a shear rate of 1 mm/min. For quantitative measurement of the viscosity of cyclohexane dispersion of UTNWs, the dispersion was characterized on a Brookfield DV-C viscometer employing a cylindrical rotator by measuring the torque imposed by the medium at different shear rates. For a frequency scan, a TA ARES-G2 rheometer was utilized by dropping a 500 mL octadecene dispersion of UTNWs onto the stage and operating the rheometer in Parallel Plate Measuring mode. Dynamic and static light scattering was carried out with an LLS spectrometer (ALV/SP-125) equipped with a solid-state He–Ne laser (output power of 22 mW at λ = 632.8 nm) and with the use of a multi-τ digital time correlator (ALV-5000).

RESULTS AND DISCUSSION

Ultrathin Nanowire (UTNW). *Conformation and Assembly.* Rare earth hydroxide UTNWs with high aspect ratio and good flexibility were obtained in excellent purity with a solvothermal hydrolysis of rare earth chlorides, as shown in the transmission electron microscopy (TEM) images of Figure 2a (GdOOH as an example). The NWs are less than 1 nm wide, highly flexible, extending in length from tens to hundreds of nanometers (usually more than 500 nm and some over 1 μm) as controlled by reaction time and temperature. They are freestanding and tend to form parallel arranged bundles with adjacent NWs with increasing concentration. As shown in figure 2b, the atomic arrangement in the high resolution transmission electron microscopy (HRTEM) image was quite disordered, resulting from the vulnerability of the UTNWs under high electron dosage and limited crystallinity under this atomic domain. The spacing between parallel NWs was 2–3 nm due to capping surfactant molecules, which gave the NWs good dispersibility in nonpolar solvent like cyclohexane. Topological features i.e. worm-like conformations and polymer-like growth mechanisms in ultrathin nanowires of Bi_2S_3 have been reported recently,[16,26] while in this system the UTNWs adopt a relatively different conformation, as the signal from dynamic/static light scattering (Figure S1) indicates a hydrodynamic radius of 34 nm and radius of gyration of 36 nm. The counterintuitive deviation might be attributed to the strong interactions between oleic acid molecules on the nanowires (Figure S2).

These 1 nm wide UTNWs showed some new features as compared to previous reports on ultrathin nanostructures.[16,17,19,26] The size reduction in inorganic cores decreased the flexural rigidity of the nanowires (which will be discussed later). As a result, the assembly behavior of the UTNWs became quite versatile, which was greatly influenced by the polarity of the solvents and the nanowire concentration. When polar solvents like ethanol are added into a diluted cyclohexane solution of UTNWs, significant bundling and coiling occur. As shown in the TEM (Figure 2c and Supporting Information Figure S3) and scanning transmission electron microscopy (STEM) images (Figure 2d and Supporting Information Figure S4), the coiling conformation of UTNW bundles led to single-loops and multiloops, both of which reduced the surface energy via van der Waals interaction between oleic acid on different UTNW segments. Different from previous reports on the coiling of nanowires, nanotubes, and nanobelts which utilized the contraction of the polymer shell[20,21] and the intrinsic charge interactions between surfaces respectively,[31,32] the driving force here comes from the ligand–ligand and ligand–solvent interactions, enabled by the flexibility of the nanowires.

Furthermore, dispersion of UTNWs in cyclohexane itself shows novel assembly behavior with increasing concentration,

dx.doi.org/10.1021/ja403471d | J. Am. Chem. Soc. 2013, 135, 11115–11124

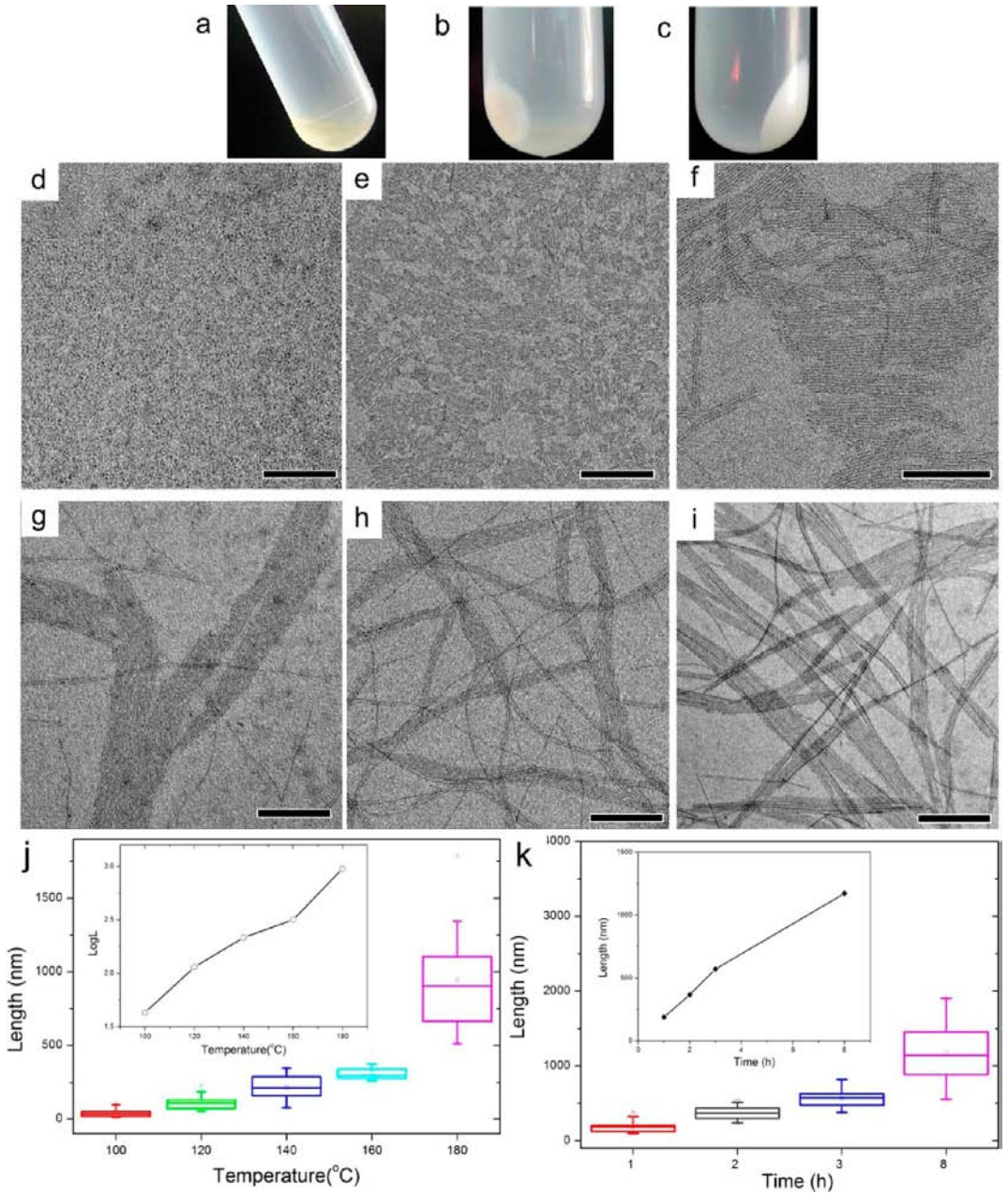

Figure 4. Typical phenomenon of product dispersion in cyclohexane with the addition of EtOH and centrifuging, respectively, in a (a) room temperature, (b) 100 °C, and (c) 120 °C or higher temperature reaction system. (d–i) TEM images of products from a reaction at room temperature, 100, 120, 140, 170, and 210 °C, respectively. The scalebars are 100 nm. Note that in panel e only TEM pictures of solid precipitate are presented; the liquid portion was almost the same as that in panel d. (j) Box chart of UTNW length distribution as a function of increasing reaction temperature. The inset is the relationship between logarithmic average length and temperature. (k) Box chart of UTNW length distribution as a function of increasing reaction time at 160 °C. The inset is the relationship between the average length and reaction time. (The box ends with 25% and 75% percentile, while the whiskers end with 5% and 95%.).

from parallel arrays, to crossed bundles, to semiperiodic porous structures with bending and entangling of the NW bundles and finally to three-dimensional (3D) porous frameworks, as shown in Figure 2e(1–4). It is interesting to note that the porous structure takes its shape within a certain concentration range (Figure 2e), similar to macromolecules which also become entangled above their "entangling concentration". (Note: this analogy was based on observation and did not have solid experimental correlation as in the reputation theory of polymers.) Although different from the real assembly structure in solution, the TEM images do give important information about the solution-phase-assembly of the NWs, which is very promising in fabricating macromolecule-like structures. In addition, thermal gravitational analysis (TGA) of the UTNWs (Supporting Information Figure S9a) indicated a weight ratio of 41.0% for the residue, equal to the inorganic ratio of 43.5% (GdOOH) in the solvent-free samples. The high ratio of organic ligands to inorganic backbones provided ligand interactions with a significant role in determining all the features of the UTNWs.

Ultrathin Nanowire (UTNW). *Physical Features.* While the NWs spontaneously formed regular microporous networks

dx.doi.org/10.1021/ja403471d | J. Am. Chem. Soc. 2013, 135, 11115–11124

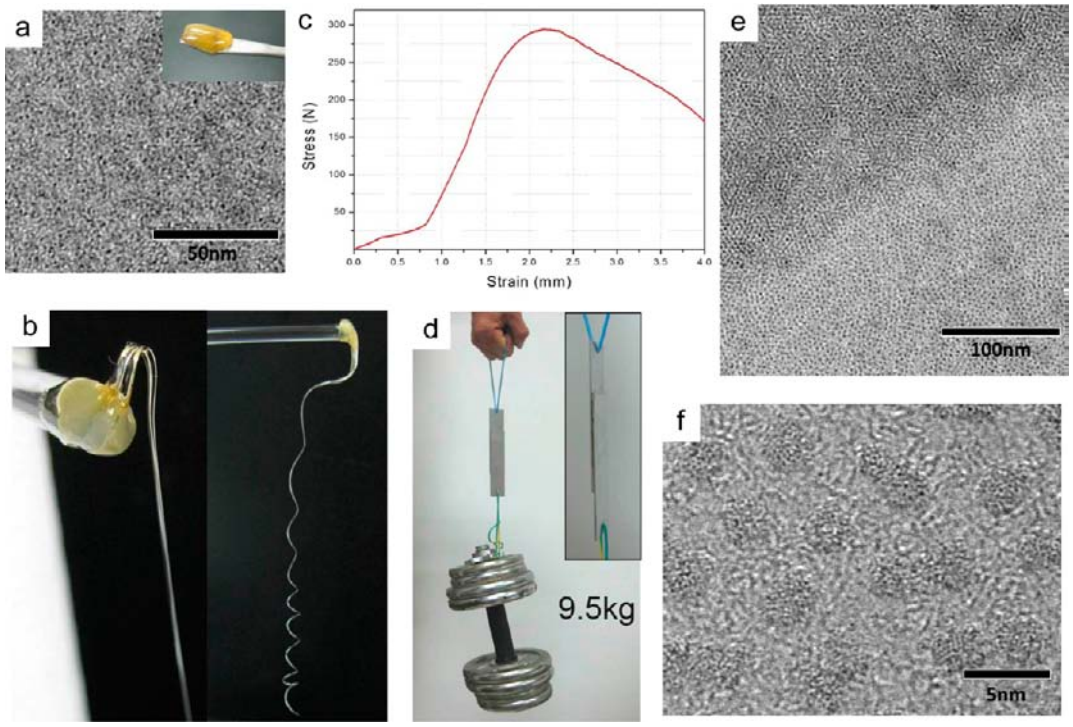

Figure 5. (a) TEM images of the as-prepared nanoclusters; the photo in the inset is its appearance. (b) Photograph of the stretched shape of the thermoplastic gel after being softened by heating and drawn (left, using $GdCl_3$, tenacious; right, using $LaCl_3$, crispy). (c) Strain−stress curve of the glue between two plates against shear. (d) Demonstration of the adhesive strength of the gel between two metal plates. (e,f) TEM and HRTEM images of zero-dimensional nanoparticles obtained through use of octadecylamine instead of oleylamine with similar reaction conditions.

of bundles, a corresponding change in the physical properties of the dispersion was observed. Phenomenally, dispersions of NWs in cyclohexane displayed high viscosity, as reflected in the sluggish movement of bubbles in cyclohexane after shaking the solution (Figure 3a). TEM images of the concentrated dispersion displayed air bubble-like structures with surfaces of consolidated NWs (Supporting Information Figure S6). Meanwhile, for a biphasic system of water and UTNW in cyclohexane, gentle shaking created stable water droplets that gathered at the interface of two liquids (Figure 3b,c), which is similar to the formation of a Pickering emulsion. Because of the entanglement of NWs around the water droplets and high viscosity in the upper phase, the water droplets were trapped without significant shrinkage even after several days. The high viscosity has also led to interesting fluidic behavior. As shown in Figure 3d, a concentrated solution displayed typical non-Newton fluid behavior with apparent shear thinning at high shear rates. Further dilution caused a change to the curve, and an interesting crossover occurred with the previous one. However, the diluted solution behaved differently with an almost constant viscosity at different shear rates, typical of a Newton fluid. The viscosity enhancement of solution in the low shear rate region might be related to the change in static assembly structures, which might be hard to visualize. It is interesting to see a crossover between the two curves. It is hypothesized that UTNWs form 3D assembly structures in cyclohexane with an entanglement of bundles of NWs: In more concentrated dispersions, the bundles increase in size and have longer relaxation times and entanglement strengths, making the shear-tore assembly structure difficult to rebuild and shear thinning more significant at high shear rates; in relatively diluted dispersions where entanglement is weak the shear thinning is less obvious. For highly concentrated solution, temporal evolution was found in rheological history by sweeping from low frequency to high frequency and back to low frequency, as is shown in Figure S6. The length and width dependence of viscosity is further illustrated in the viscosity measurement of diluted cyclohexane dispersions of UTNWs (Figure 3e). The relative viscosity measured with an Ubbelohde viscometer peaked around 180 °C while the length of the UTNWs increased with temperature below this point and the width of the UTNWs increased with the temperature above it.

In addition, the assembly structure and the high viscosity led to solvent confinement and solidification of the dispersion. It was found that a concentrated dispersion of UTNWs in cyclohexane gradually solidified, forming a transparent organo-gel after aging for a few days (Figure 3f). This might be caused by a structured-fluid induced solvent ordering: Consolidated frameworks of NW bundles provided a confined space where solvent molecules became arrested because of solvent/ligand interactions, while limited evaporation further enhanced the NW relaxation, solvent arresting, and gel formation. Depletion-induced gelation of colloidal dispersions has been investigated for a long time,[33−35] and the process typically led to a large concrete aggregation with dimensional features in micrometers as a result of phase-separation,[34] whereas transparent organo-gels were still hard to obtain from an inorganic nanostructure system. In a recent report, a hybrid inorganic-nanocrystal/polymer transparent hydrogel was obtained through photo-initiated grafting and cross-linking of organic monomers over semiconductor nanocrystals.[36] However, the organo-gel mentioned here was different from the one in that report as the building units comprised 1D UTNWs and no additional organic linkers were used. Actually, considering the similarity in size and conformations, the cross-linking and gelation behavior of the UTNWs could be compared with that of polymeric

dx.doi.org/10.1021/ja403471d | J. Am. Chem. Soc. 2013, 135, 11115−11124

molecules with side-chain supramolecular interactions.[37] The gelation typically occurred in organic solvents such as cyclohexane, hexane, toluene, etc., and could be further accelerated with the introduction of weak organic acids like naphthylacetic acid, as is shown in Figure 3g,h. With naphthylacetic acid added, gelation could take place within seconds at extremely low concentrations of 0.1% by weight percentage of NW to solution. This might be related to the protonation and removal of some surface ligands and exposure of the inorganic core; these exposed sites were very unstable and preferred to cross-link with other exposed sites and the gelation happened within seconds, resulting in a transparent gel. A TEM image prepared from this crushed gel was shown in Supporting Information Figure S8, showing the intimately cross-linked network of nanowires.

Ultrathin Nanowire (UTNW). *Growth from Nanoclusters.* The flexible ultrathin nanowires were found to be constructed from ultrafine nanoclusters according to results with different reaction times. The nanoclusters were obtained at the initial stage of reaction and appeared as 1 nm nanoparticles (NP) in TEM images in Figure 4d. Previous research on the growth mode of nanowires from anisotropic assembling of nanocrystals indicated an "oriented attachment" mechanism, which possibly can be introduced here.[38−42] Actually, for the 1-D UTNW, progressive growth of the wire was fully illustrated by the morphology change of the products with increasing reaction time or reaction temperature. According to the TEM results of the products from a series of 4 h reaction systems at different temperatures in Figure 4d−i and our statistics on the length-temperature relationship in Figure 4j, very short ultrathin NWs began to emerge between 80 and 100 °C reactions, and the length gradually increased while the width remained almost constant up to 170 °C −180 °C; the length in the logarithmic form takes a near-linear relationship with respect to temperature. Similarly, when plotting the NW length together with increasing reaction time at a constant temperature of 160 °C (Figure 4k), a quasi-linear relationship can be found, showing a stepwise growth mode. The growth mode of the UTNWs (Figure 1b) was very similar to the traditional polymerization of organic monomers (Figure 1a), like styrene, not only in form but also in size. The degree of "polymerization" was estimated to be 500−1000 assuming a 1 nm sized spherical nanocrystal monomer which links to form a nanowire as long as 500−1000 nm. An even higher reaction temperature will cause the coarsening of the UTNWs into some robust NWs which is ca. 3 nm wide and high in crystallinity, while the diffraction peaks were very weak for those fabricated under 180 °C indicating poor crystallinity, as shown in Supporting Information Figure S9.

In addition, the monomers themselves were thermoplastic and formed a highly viscous gel, which can be drawn into tenacious silk, as shown in Figure 5b left. (Replacing $GdCl_3$ with $LaCl_3$ leads to spiral-shaped fragile silk, as shown in Figure 5b right.) After the cyclohexane dispersion is dried by using a heating−cooling process, the product can be used as a high-strength adhesive. The binding strength of the gel pasted between two metal plates can hold a 9.5 kg dumbbell and withstand many cycles of lifting and unloading, as shown in Figure 5d; A shear-force measurement provided the fracture stress of nearly 300N (Figure 5c). This excellent mechanical property was attributed to the strong interaction between the tiny nanoparticles.

Ultrathin Nanoribbon (UTNR). *Conformational Diversity.* The process of nanocluster assembly is also seen in various ultrathin nanoribbon-(or nanosheet)-based morphologies of $Y(OH)_3$. Figure 6 demonstrated the various modifications that

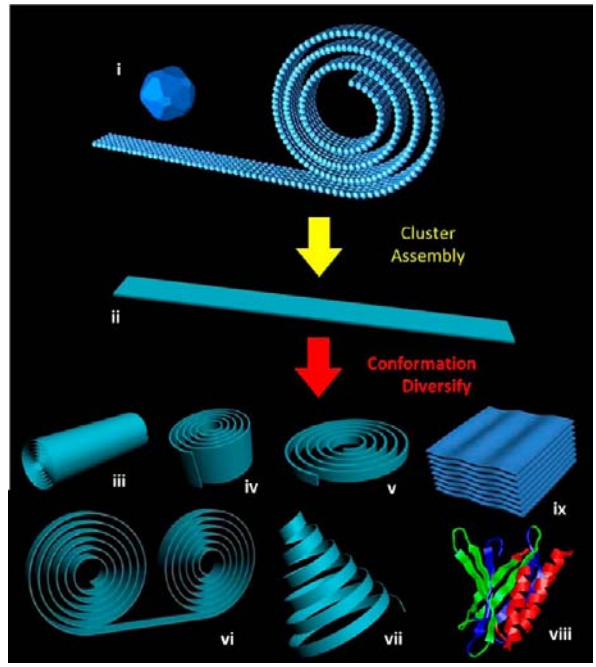

Figure 6. Schematic of 2D cluster-assembly and possible variations in the UTNR conformation. Each model here has a corresponding nanostructure in the TEM images in Figure 7. (Note: The last model (viii) is the ribbon model of the protein structure of 3N8B *Borrelia burgdorferi* Pur-alpha.[49])

can be made to this prototype 2D assembly. The rich variety came from the ultrathin thickness of 2D assembly nanostructures (nanosheets and nanoribbons) which decreased to around 1 nm. In this case, the shape of the inorganic backbone was overwhelmed by the interactions between ligands and the solvent, which is similar to its 1D NW counterpart. Various conformational changes from one single nanostructure or stacking-up of multiple nanostructures can be controllably fabricated. In the case of $Y(OH)_3$, this includes flat nanoribbons, half-rolled nanoribbons, nanorolls, nanospirals, stacked sheet-arrays, and other complex structures, as summarized in the series of models in Figure 6. The final conformations of these nanostructures were determined by the energy competition between inorganic rigidity and ligand interactions, which can be tuned by using different reaction conditions. Rolling of the prototype nanoribbons decreased the energy of the conformation by increasing the van der Waals interaction between the organic ligands at the cost of bending energy increase of the inorganic framework. Generally, there are three different ways of conformation tuning: (1) coiling degree, (2) aspect ratio (AR), and (3) stacking structure.

First, it was found that the coiling degree of the UTNRs typically decreases with increasing reaction time and temperature, which evolves through a series of typical conformations with decreasing coiling degree as shown in Figure 7d back to Figure 7a. In short-time products, the complete self-coiling structure in Figure 7d is preferred after the 2D assembly of nanoclusters, as energy gain from van der Waals interactions of ligand molecules surpasses the bending energy cost of the

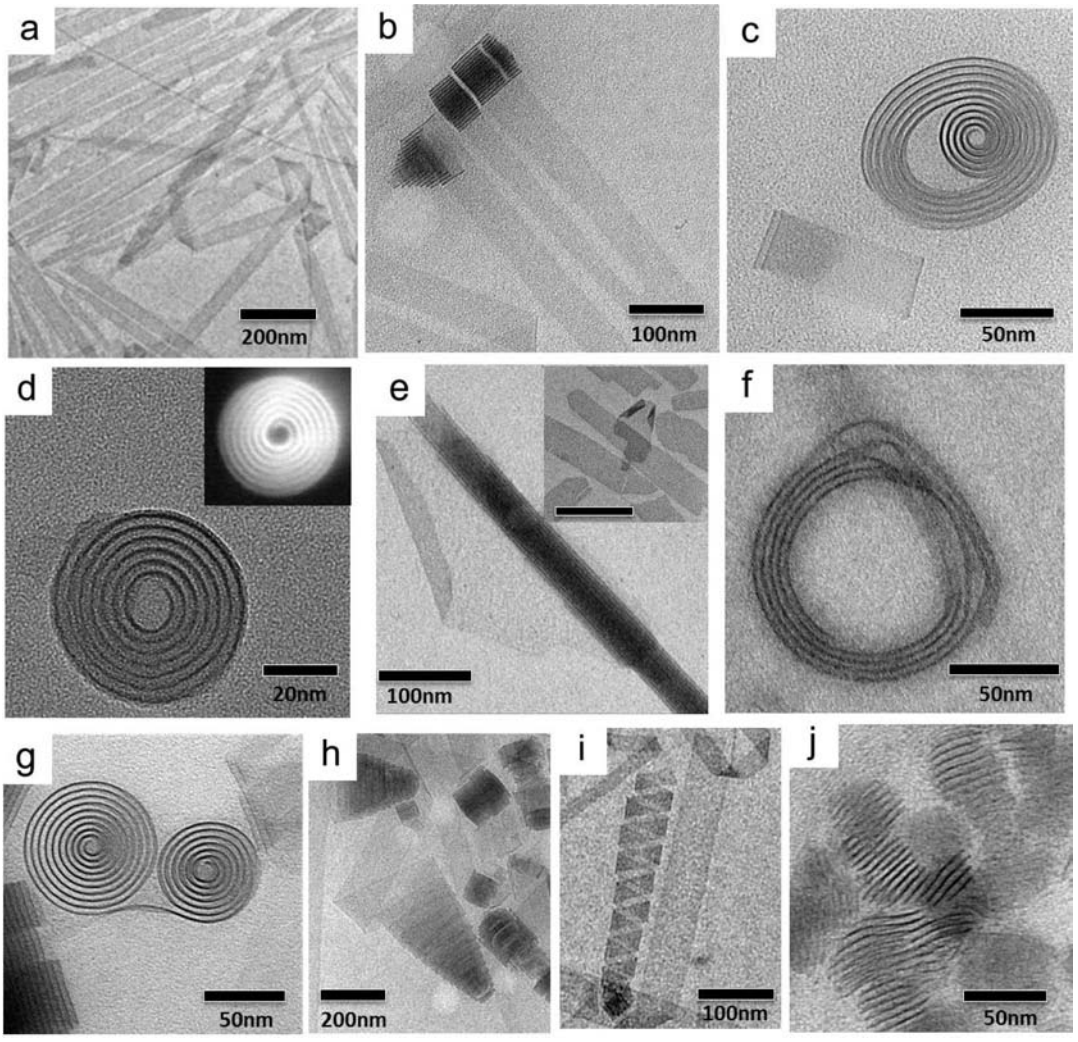

Figure 7. Various conformational derivatives of 2D ultrathin nanostructured $Y(OH)_3$. (a–d) TEM images of UTNR with varying degrees of coiling: (a) flat nanoribbons, (b) one-end rolled nanoribbons, (c) partially extended nanorolls as compared to (d) the fully coiled nanoroll, all of which can be tuned by changing reaction time; the inset of image d shows the corresponding STEM image of the nanoroll. (e) TEM image of a high-AR elongated nanoroll with a little rim laying on the substrate folded; the inset shows the short-time product, that is, flat ultrathin nanofilms which fold into nanorolls with increasing reaction time. (f) TEM image of a low-AR disk-like nanorolls. (g–i) TEM images of (g) twin nanorolls, (h) involute nanospirals, and (i) nanohelixes. (j) TEM image of stacked few-layer ultrathin nanosheets synthesized by replacing oleic acid with steric acid.

inorganic backbones due to low rigidity of the nanoribbons. With the prolonging of reaction time, the rigidity increases and the nanoribbons gradually stretch out and finally became flat (Figure 7a). The decoiling process involved multiple steps: nanorolls were first broken apart between certain adjacent layers (Figure 7c) and the outer layers quickly flattened with the central part still in rolled form (Figure 7b). The four typical stages of conformations, as shown in Figure 7, a–d were further supported by Figure 8 with large scale TEM images of the overall conformational changes in the products. As previously mentioned, conformation change came from the energy balance; the reaction-time-dependent conformational variation was accompanied by continuous structure change and rigidity increase, as shown by the X-ray diffraction patterns of the series of samples (Supporting Information, Figure S10). All products can be indexed to the pattern of $Y(OH)_3$ (JCPDS 21-1447), while a monotonous variation in main peaks, especially the ⟨110⟩ peak shrinking and ⟨114⟩ rising, follows the conformation change from perfect nanorolls to half decoiled and fully decoiled flat ribbons, as shown in Figure 8. Minor surfactant OM in this system served as some kind of retardant in addition to hydrolyzing alkaline as the decoiling process slowed down with increasing OM amount.

Second, when it comes to AR, the shape of the nanorolls can be squeezed or elongated by tuning the OA/OM ratio. Actually, medium AR nanorolls in Figure 7d were obtained in a system with high OA and low OM (2.7g/0.8g), and high AR nanorolls in Figure 6e were obtained with a low-OA and high-OM system (0.4g/2.7g) while low AR nanorolls shown in Figure 6f came from a low-OA low-OM system (0.9g/0.5g). The detailed mechanism for the roll of OA/OM was unclear, but it should be related to the synergetic soft-templating effect of the OA and OM in ethanol. Interestingly, although medium AR nanorolls display a decoiling process with increasing reaction time and finally become flat nanoribbons, high AR nanorolls have an opposite time dependency—short-time reaction leads to flat stretching nanofilms while increasing reaction time initiates the rolling-up (Figure 7e and Supporting Information, Figure S11). The intermediate product for this rolling transformation can also be seen in Supporting

dx.doi.org/10.1021/ja403471d | J. Am. Chem. Soc. 2013, 135, 11115–11124

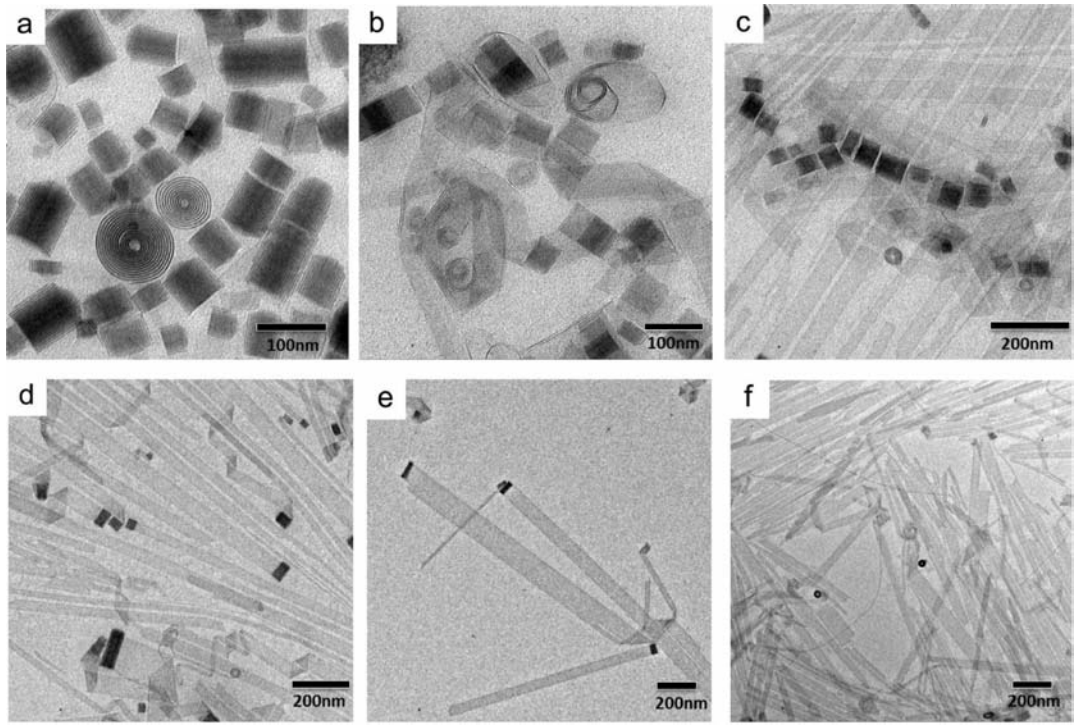

Figure 8. TEM images of products from an identical prepared reaction system (3.0 mL OA/0.8g OM/0.15g YCl_3) heated with increasing time and temperature (a) 170 °C for 6 h, 180 °C for (b) 6 h, (c) 8 h, (d,e) 12 h, and (f) 200 °C for 3 h. These images show the typical conformation changes in the decoiling process. Although three different temperature values were adopted rather than constant temperature with increasing reaction time, it was just for convenience and should make no difference as compared to the series with increasing time at constant temperature.

Information, Figure S12 with some nanoclusters still remaining in the background (without separation prior to TEM). Similar to the case of medium-AR nanorolls where more OM leads to slow decoiling, the coiling process of high-AR nanorolls was slowed down by increasing the amount of OA. Also, the coiling process of the high AR nanorolls was found to be related to the variation in the inorganic structure, as shown in the reaction-time-dependent XRD pattern changes (Figure S13).

Third, as the conformations are determined by the interaction between ligands on the surface of nanoribbons, changing the ligands could bring about differences. The formation of nanoribbon and nanoroll series depends on certain kinds of aliphatic amines. When straight-chain octadecylamine or butylamine was used in place of V-shaped oleylamine; a similar result was obtained. However, the products became UTNWs when branched-chain alkylamine and dialkylamine was used due to a hindrance effect. On the other hand, when the V-shaped OA molecules were replaced by the straight-chain C18 steric acid molecules, arrays of ultrathin nanosheets were obtained, as shown in Figure 7j. It is intuitive to hypothesize that the specific shape and alignment of ligand molecules on the 2D nanoribbon/nanosheet surface has additional effects on the rolling tendency. However, with other straight-chain aliphatic acids with shorter chains of C10, C12, C14, C16, the cluster was poorly protected against assembly, and the product consisted of micrometer-sized agglomerates and large-area films.

In addition, other complex conformations were also easily identifiable from the reaction systems with proper ligand combinations which include the double coiling nanorolls, involute nanospirals, and nanohelixes, as shown in Figure 7g, 7h, and 7i, with their corresponding models depicted in the bottom line of Figure 6. Similar phenomena of shape selection of nanoribbons have also been discovered in many biological systems induced by interaction between molecular segments.[43,44] The ultrathin thickness, significantly reduced rigidity of the inorganic backbone, and rich selection of ligand library has given rise to the prevailing interaction of the surface ligands and the conformational diversity and tunability of the products.

■ FURTHER DISCUSSIONS

The surface (ligand) properties have significant influence on the behavior of the ultrathin nanostructures, and the interactions between ligands of different nanostructures and between ligands and surrounding solvent finally determine the conformations and the assembly structure. However, the influence is not obvious in traditional 1D nanostructures because their intrinsic flexural rigidity results in an energy barrier too high for the van der Waals interactions between ligand and solvent/ligand interactions to take effect. In this case, assembly was most seen with the regular arrangement of nanostructures. Through the reduction of size and increased ratio of ligand to inorganic backbone, different conformations and assembly structures can be constructed from these long building units, including nanoloops, periodic frameworks from UTNWs, and various coiling conformations in UTNRs.

A simplified model for the formation of nanorolls from nanoribbons was introduced here for better intuitive understanding. Typically, the rolling of a perfectly elastic thin plate involves a strain energy cost $E_{str} = Dk^2/2$ (The exact expression of E_{str} for the whole nanoroll should involve the integral form $\int Dk^2/2$ along the nanoroll) where k stands for the curvature and D stands for flexural rigidity;[45] The flexural rigidity is related to the Young's modulus, Y, thickness, h, and Poisson's ratio, ν, in the relationship of $D = Yh^3/12(1 - \nu^2)$.[46] Although Y

dx.doi.org/10.1021/ja403471d | J. Am. Chem. Soc. 2013, 135, 11115−11124

may have a different size-scaling law between different materials[47,48] and typically increases as size is reduced due to surface stiffening, D is more dependent on the thickness h with a cubic law. Therefore, ultrathin nanostructures reduce the rigidity of the material and lower the bending energy into a level comparable to other microscopic interactions, like electrostatic and van der Waals interactions, etc. In this case, bending not only involves strain energy cost but also brings about energy gain from the van der Waals interaction between opposing surfactant layers on the surface of the ultrathin nanoribbons which is $E_{van} = \sigma^* A(R)$ where $A(R)$ stands for the opposing area as a function of radius and σ is the van der Waals interaction between unit area of monolayers of oleic acid (oleylamine). Obviously, as E_{str} scales with the square of the curvature, higher strain energy is accumulated when the nanoroll contracts. On the other hand, more van der Waals energy is obtained by shrinking the roll and increasing the opposing areas as the exposed outermost and innermost surfaces of the nanoroll were reduced. Equilibrium conformation holds when the energy balance is reached between E_{str} and E_{van}. A similar treatment also applies to the UTNWs for the formation of multiloops and periodic assembly structures.

CONCLUSION

In summary, the ultrafine size of nanostructure units has endowed them with assembly macromolecule-like properties while the inorganic backbone provided the unique properties unavailable in traditional macromolecules. Magnetic, optical, and other properties can be integrated into these materials by carefully selecting the inorganic substrate materials,[28] and mechanical properties can be tuned through the choice of organic ligands and solvent. This might also provide a new way to fabricate flexible devices, for example, to enhance the lighting efficiency of OLED devices. In our case, the GdOOH and EuOOH both kept their intrinsic features in superparamagnetism and fluorescence after size minimizing (although the OH group limits the fluorescence intensity), as shown in Supporting Information, Figure S14 and S15. On the other hand, control over the ligand interaction changes the microscopic conformation and hence macroscopic mechanical performance of the materials. Further exploration of a similar system may extend current work to provide more excellent combinations of typical properties of inorganic and organic materials.

ASSOCIATED CONTENT

Supporting Information

Light scattering, FTIR, XRD, thermal analysis, and additional TEM, STEM, rheological, and magnetic data for UTNWs; additional TEM, XRD, and fluorescence spectrum for UTNRs. This material is available free of charge via the Internet at http://pubs.acs.org.

AUTHOR INFORMATION

Corresponding Author

wangxun@mail.tsinghua.edu.cn

Notes

The authors declare no competing financial interest.

ACKNOWLEDGMENTS

This work was supported by NSFC (91127040, 21221062), and the State Key Project of Fundamental Research for Nanoscience and Nanotechnology (2011CB932402).

REFERENCES

(1) Morales, A. M.; Lieber, C. M. *Science* **1998**, *279*, 208−211.
(2) Thess, A.; Lee, R.; Nikolaev, P.; Dai, H.; Petit, P.; Robert, J.; Xu, C.; Lee, Y. H.; Kim, S. G.; Rinzler, A. G.; Colbert, D. T.; Scuseria, G. E.; Tománek, D.; Fischer, J. E.; Smalley, R. E. *Science* **1996**, *273*, 483−487.
(3) Bruchez, M.; Moronne, M.; Gin, P.; Weiss, S.; Alivisatos, A. P. *Science* **1998**, *281*, 2013−2016.
(4) Murray, C. B.; Norris, D. J.; Bawendi, M. G. *J. Am. Chem. Soc.* **1993**, *115*, 8706−8715.
(5) Pan, Z. W.; Dai, Z. R.; Wang, Z. L. *Science* **2001**, *291*, 1947−1949.
(6) Sun, Y. G.; Xia, Y. N. *Science* **2002**, *298*, 2176−2179.
(7) Wang, X.; Zhuang, J.; Peng, Q.; Li, Y. D. *Nature* **2005**, *437*, 121−124.
(8) Yuan, J.; Xu, Y.; Muller, A. H. E. *Chem. Soc. Rev.* **2011**, *40*, 640−655.
(9) Soler-Illia, G. J. A. A.; Azzaroni, O. *Chem. Soc. Rev.* **2011**, *40*, 1107−1150.
(10) Qi, W.; Wu, L. *Polym. Int.* **2009**, *58*, 1217−1225.
(11) Ruiz-Hitzky, E.; Aranda, P.; Darder, M.; Ogawa, M. *Chem. Soc. Rev.* **2011**, *40*, 801−828.
(12) Herman, D. J.; Goldberger, J. E.; Chao, S.; Martin, D. T.; Stupp, S. I. *ACS Nano* **2010**, *5*, 565−573.
(13) Haraguchi, K.; Takehisa, T. *Adv. Mater.* **2002**, *14*, 1120−1124.
(14) Gülseren, O.; Ercolessi, F.; Tosatti, E. *Phys. Rev. Lett.* **1998**, *80*, 3775−3778.
(15) Hong, B. H.; Bae, S. C.; Lee, C.-W.; Jeong, S.; Kim, K. S. *Science* **2001**, *294*, 348−351.
(16) Cademartiri, L.; Malakooti, R.; O'Brien, P. G.; Migliori, A.; Petrov, S.; Kherani, N. P.; Ozin, G. A. *Angew. Chem., Int. Ed.* **2008**, *47*, 3652−3652.
(17) Huo, Z. Y.; Tsung, C. K.; Huang, W. Y.; Zhang, X. F.; Yang, P. D. *Nano Lett.* **2008**, *8*, 2041−2044.
(18) Huo, Z. Y.; Tsung, C. K.; Huang, W. Y.; Fardy, M.; Yan, R. X.; Zhang, X. F.; Li, Y. D.; Yang, P. D. *Nano Lett.* **2009**, *9*, 1260−1264.
(19) Du, Y. P.; Zhang, Y. W.; Yan, Z. G.; Sun, L. D.; Yan, C. H. *J. Am. Chem. Soc.* **2009**, *131*, 16364−16365.
(20) Xu, J.; Wang, H.; Liu, C.; Yang, Y.; Chen, T.; Wang, Y.; Wang, F.; Liu, X.; Xing, B.; Chen, H. *J. Am. Chem. Soc.* **2010**, *132*, 11920−11922.
(21) Chen, L.; Wang, H.; Xu, J.; Shen, X.; Yao, L.; Zhu, L.; Zeng, Z.; Zhang, H.; Chen, H. *J. Am. Chem. Soc.* **2011**, *133*, 9654−9657.
(22) Zhu, G. X.; Zhang, S. G.; Xu, Z.; Ma, J.; Shen, X. P. *J. Am. Chem. Soc.* **2011**, *133*, 15605−15612.
(23) Wang, Y.; Wang, Q.; Sun, H.; Zhang, W.; Chen, G.; Wang, Y.; Shen, X.; Han, Y.; Lu, X.; Chen, H. *J. Am. Chem. Soc.* **2011**, *133*, 20060−20063.
(24) Du, Y.; Yin, Z.; Zhu, J.; Huang, X.; Wu, X.-J.; Zeng, Z.; Yan, Q.; Zhang, H. *Nat. Commun.* **2012**, *3*, 2181.
(25) Huang, X.; Li, S.; Wu, S.; Huang, Y.; Boey, F.; Gan, C. L.; Zhang, H. *Adv. Mater.* **2012**, *24*, 979−983.
(26) Cademartiri, L.; Guerin, G.; Bishop, K. J. M.; Winnik, M. A.; Ozin, G. A. *J. Am. Chem. Soc.* **2012**, *134*, 9327−9334.
(27) Thomson, J. W.; Cademartiri, L.; MacDonald, M.; Petrov, S.; Calestani, G.; Zhang, P.; Ozin, G. A. *J. Am. Chem. Soc.* **2010**, *132*, 9058−9068.
(28) Wang, P.-p.; Yang, Y.; Zhuang, J.; Wang, X. *J. Am. Chem. Soc.* **2013**, *135*, 6834−6837.
(29) Hu, S.; Wang, X. *Chem. Soc. Rev.* **2013**, *42*, 5577−5594.
(30) Cademartiri, L.; Scotognella, F.; O'Brien, P. G.; Lotsch, B. V.; Thomson, J.; Petrov, S.; Kherani, N. P.; Ozin, G. A. *Nano Lett.* **2009**, *9*, 1482−1486.
(31) Kong, X. Y.; Ding, Y.; Yang, R.; Wang, Z. L. *Science* **2004**, *303*, 1348−1351.
(32) Kong, X. Y.; Wang, Z. L. *Nano Lett.* **2003**, *3*, 1625−1631.
(33) Buzzaccaro, S.; Rusconi, R.; Piazza, R. *Phys. Rev. Lett.* **2007**, *99*, 098301.

(34) Lu, P. J.; Zaccarelli, E.; Ciulla, F.; Schofield, A. B.; Sciortino, F.; Weitz, D. A. *Nature* **2008**, *453*, 499−503.
(35) Zaccarelli, E. *J. Phys.: Condens. Matter* **2007**, *19*, 323101.
(36) Zhang, D.; Yang, J.; Bao, S.; Wu, Q.; Wang, Q. *Sci. Rep.* **2013**, *3*, 1399.
(37) Yan, X.; Wang, F.; Zheng, B.; Huang, F. *Chem. Soc. Rev.* **2012**, *41*, 6042−6065.
(38) Banfield, J. F.; Welch, S. A.; Zhang, H. Z.; Ebert, T. T.; Penn, R. L. *Science* **2000**, *289*, 751−754.
(39) Tang, Z.; Kotov, N. A.; Giersig, M. *Science* **2002**, *297*, 237−240.
(40) Cho, K. S.; Talapin, D. V.; Gaschler, W.; Murray, C. B. *J. Am. Chem. Soc.* **2005**, *127*, 7140−7147.
(41) Cölfen, H.; Antonietti, M. *Angew. Chem., Int. Ed.* **2005**, *44*, 5576−5591.
(42) Ribeiro, C.; Lee, E. J.; Longo, E.; Leite, E. R. *Chemphyschem* **2006**, *7*, 664−670.
(43) Cui, H.; Muraoka, T.; Cheetham, A. G.; Stupp, S. I. *Nano Lett.* **2009**, *9*, 945−951.
(44) Selinger, R. L. B.; Selinger, J. V.; Malanoski, A. P.; Schnur, J. M. *Phys. Rev. Lett.* **2004**, *93*, 158103.
(45) Patra, N.; Song, Y.; Král, P. *ACS Nano* **2011**, *5*, 1798−1804.
(46) Landau, L. D.; Lifshitz, E. M. *Theory of Elasticity*, 3rd ed.; Butterworth−Heinemann: Oxford, 1986; *Vol. 7*, pp 46−53.
(47) Chen, C. Q.; Shi, Y.; Zhang, Y. S.; Zhu, J.; Yan, Y. J. *Phys. Rev. Lett.* **2006**, *96*, 075505.
(48) Nam, C.-Y.; Jaroenapibal, P.; Tham, D.; Luzzi, D. E.; Evoy, S.; Fischer, J. E. *Nano Lett.* **2006**, *6*, 153−158.
(49) Graebsch, A.; Roche, S.; Kostrewa, D.; Söding, J.; Niessing, D. *PLoS ONE* **2010**, *5*, e13402.